Research Article Vol. 38, No. 4 / April 2021 / Journal of the Optical Society of America B 1229

Journal of the Optical Society of America B

OPTICAL PHYSICS

Production of ^{23}Na Bose–Einstein condensates in the $F = 2$ state using D_2 gray molasses

Zhenlian Shi,[1,2] Ziliang Li,[1,2] Pengjun Wang,[1,2,*] Khan Sadiq Nawaz,[1,2] Liangchao Chen,[1,2] Zengming Meng,[1,2] Lianghui Huang,[1,2] and Jing Zhang[1,2,3,4]

[1]State Key Laboratory of Quantum Optics and Quantum Optics Devices, Institute of Opto-Electronics, Shanxi University, Taiyuan, Shanxi 030006, China
[2]Collaborative Innovation Center of Extreme Optics, Shanxi University, Taiyuan, Shanxi 030006, China
[3]e-mail: jzhang74@sxu.edu.cn
[4]e-mail: jzhang74@yahoo.com
*Corresponding author: pengjun_wang@sxu.edu.cn

Received 24 November 2020; revised 24 January 2021; accepted 1 March 2021; posted 2 March 2021 (Doc. ID 414781); published 22 March 2021

We report on the production of Bose–Einstein condensates of sodium atoms in the hyperfine state $|F = 2, m_F = 2\rangle$ in a crossed optical dipole trap using D_2 gray molasses. We use the gray molasses sub-Doppler cooling technique to obtain an atomic sample of 3×10^8 at 56 μK. After the radio frequency (RF) evaporation cooling in an optically plugged magnetic trap, we transfer the atoms sample of 2.5×10^6 at 5.7 μK to a crossed optical dipole trap where a pure condensate with an atom number of 2×10^5 and lifetime of 6.3 s is obtained by further evaporation. We compare the cooling process of sodium atoms in the $|2, 2\rangle$ and the $|1, 1\rangle$ states by evaporation in the optical trap, and also observe the different three-body loss rates by the lifetime measurement.

https://doi.org/10.1364/JOSAB.414781

1. INTRODUCTION

Ultracold atomic gases offer a remarkably rich platform [1] for a wide range of applications, such as coherent manipulation of strongly correlated many-body states in optical lattices [2–5], quantum simulation of spin orbit coupling [6–9], and association of ultracold atoms into molecules in the absolute ground state to study the long range dipole–dipole interaction and ultracold chemistry [10,11]. To obtain atomic samples with a higher number and a lower temperature, different special cooling routes are designed, because there are different collision properties for atoms in different hyperfine states during different temperature regimes, especially in the creation of ultracold atomic mixtures [12–18].

The ultracold atoms of ^{23}Na are of particular interest because of its special collision property. The spinor Bose–Einstein condensates (BECs) of ^{23}Na atoms are intensively studied due to the antiferromagnetic nature of the ^{23}Na atoms in the $F = 1$ ground state [19,20]. Theoretical models involving the spin-2 spinor condensates have predicted richer quantum phenomena as compared to the spin-1 spinor condensates [21–23] but the unfavorable three body losses makes it difficult to cool the atoms directly in the spin-2 state [24,25]. In the study of ultracold chemistry, ^{40}K^{23}Na is one of the chemically stable fermionic ground state molecules that has been produced [26]; the other one being ^{40}K^{133}Cs [27]. The simultaneous cooling of the mixture of ^{40}K and ^{23}Na, however, is a complex process due to the high three-body loss rate and large background scattering length [28]. Therefore, we must cool ^{40}K sympathetically using ^{23}Na in the ground state $|2, 2\rangle$ initially in the magnetic trap and then transfer the ^{23}Na atoms to $|1, 1\rangle$ in the optical trap to prevent the higher three-body loss rate at a lower temperature [29]. A recent study [30] has reported the sympathetic cooling of ultracold molecules ^{23}Na^{6}Li in a triplet ground state by ^{23}Na atoms in the $|2, 1\rangle$ state and it was found that the $|1, 1\rangle$ state atoms were not able to cool the molecules [14].

As mentioned in [24], cooling sodium atoms in the $F = 2$ state is more difficult than in the $F = 1$ state due to the higher three-body loss rate in the $F = 2$ state. The three-body loss rate of sodium atoms in the $F = 2$ state is about 1.6×10^{-29} cm^6/s, which is one order of magnitude higher than for the atoms in the $F = 1$ state. In the previous works, the BEC of sodium atoms in the $F = 2$ state were realized by transferring the population from the $F = 1$ state BECs using microwave transition. Till this date, we are unaware of the experimental report about direct cooling of sodium atoms in the $F = 2$ state to BEC in the optical trap.

In this work, we report on the experimental production of BEC of sodium atoms in the $F = 2$ state. We take advantage of the gray molasses on the D_2 line, as reported in our previous work [31], to obtain the sufficient initial loading of the quadrupole magnetic trap in the $|F = 2, m_F = 2\rangle$ state. After a RF-induced forced evaporative cooling in the optically plugged magnetic trap, around 2.5×10^6 atoms at a temperature of

5.7 μK are transferred to a crossed optical trap. Then, an optimized evaporation process in the optical trap is used to generate a pure BEC of sodium atoms in the spin polarized $|F=2, m_F=2\rangle$ state. We also study the different collision properties of sodium atoms in the $|2, 2\rangle$ and the $|1, 1\rangle$ states, and measure the different three-body loss rates.

2. MAGNETO-OPTICAL TRAP

The experimental system consists of two vacuum chambers: One is a metallic chamber made of stainless steel 316L for a two-dimensional magneto-optical trap (2D MOT) and the other one is an ultrahigh vacuum glass cell (called the science chamber) made of fused silica with external antireflection coating (for the wavelengths of interest), where the 3D MOT and BEC are realized, as shown in Fig. 1.

Our experiment starts by collecting ^{23}Na atoms in a 2D MOT made by neodymium bar permanent magnets [32], which generate a magnetic field for both the 2D MOT and Zeeman slower in the gravity direction (-z direction). This design has been used to achieve a high atomic flux of ^{6}Li [33] and ^{23}Na [34] atoms, offering a more compact geometry compared to the standard Zeeman slower. The hot atoms released from the heated oven (∼200°C) move along the z direction and are decelerated by a Zeeman slower beam with a red detuning of 309 MHz from the $|F_g=2\rangle \rightarrow |F_e=3\rangle$ transition, which enter the vacuum chamber from the Zeeman slower beam window linearly polarized along the x direction. Then, the atoms are collected by the 2D MOT and sent to the ultrahigh vacuum science chamber by a blue-detuned (from the $|F_g=2\rangle \rightarrow |F_e=3\rangle$ transition) push beam along the x direction. There are several advantages of this scheme, such as a smaller size, low sodium source consumption to maintain efficient loading of the MOT, and better background pressure in the science chamber because the atoms from the oven cannot enter directly into the science chamber through the differential tube. Moreover, an improved 2D MOT based on this scheme

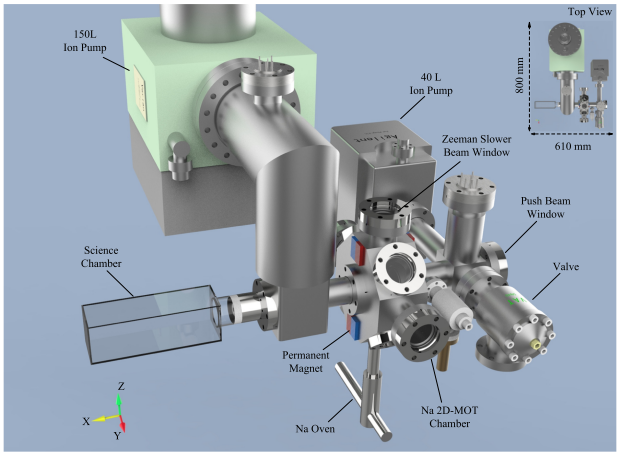

Fig. 1. Schematic drawing of the vacuum system designed for the production of ultracold sodium atoms, consisting of the 2D MOT and 3D MOT. The sodium source is located 200 mm below from the center of the 2D MOT and the atoms from this source are slowed down and loaded into the 2D MOT by the Zeeman slower. The inset shows the top view of the whole vacuum system with dimensions of about 800 mm × 610 mm.

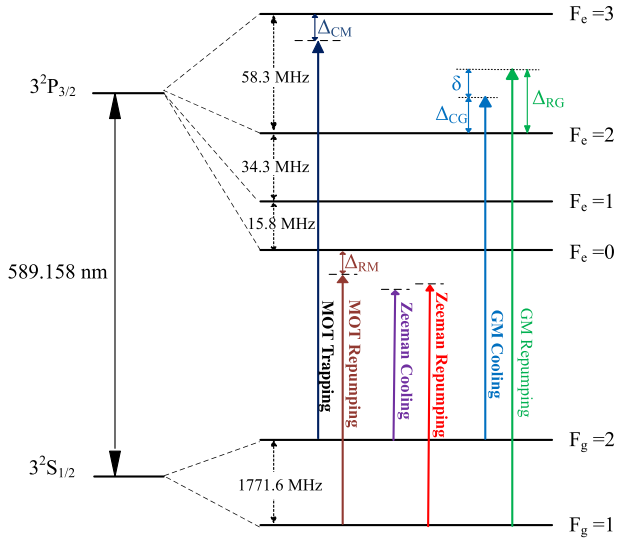

Fig. 2. Energy level diagram of ^{23}Na atom and the optical transitions used for the 3D MOT, gray molasses cooling, and Zeeman slower. The δ denotes the two-photon Raman detuning.

has been developed by [35] to increase the atomic flux by using multiple-sideband cooling in the 2D MOT.

In the science chamber, the atoms are trapped and cooled by the six 3D MOT beams forming the dual-operation magneto-optical trap operating on the D_2 transition [36]. Each of these six beams carry two laser frequencies: One is marked as the MOT trapping light and is tuned to $|F_g=2\rangle \rightarrow |F_e=3\rangle$ transition with a red detuning of 41 MHz, and the other, called the MOT repumping light, is tuned to the $|F_g=1\rangle \rightarrow |F_e=0\rangle$ transition (in contrast to the typical repump locking transition $|F_g=1\rangle \rightarrow |F_e=2\rangle$) with a red detuning of 6 MHz, as shown in Fig. 2. Actually, the roles of the cooling and repumping frequencies are not distinct because there are the almost same number of atoms in $F=1$ and $F=2$ ground state in the 3D MOT. A low magnetic field with a gradient of 2.7 G/cm along the z direction is used to keep the atomic density and hence the laser-induced atomic loss low. The total number of atoms trapped in the 3D MOT is about 7×10^9 at 700 μK.

3. GRAY MOLASSES ON THE D_2 LINE

Gray molasses (GM) cooling is a special method for sub-Doppler laser cooling, which consists of polarization gradient cooling and velocity-selective coherent population trapping [37]. The GM cooling mechanism operates on the dark and bright states, which are the coherent superposition of the Zeeman sublevels in the ground hyperfine manifold $F_g=1$ and $F_g=2$. In the $\sigma^+-\sigma^-$ configuration, the stationary wave formed by the molasses laser beams has a linear polarization that rotates around the beam direction in a linear helical pattern with a period of one wavelength λ. In this configuration, the polarization gradient of the light field changes without a change in the ellipticity (as opposed to the $lin\perp lin$ configuration). The moving atom in the rotating linear polarization vector faces a fictitious homogeneous magnetic field in the direction of motion, which resembles a friction force [38,39]. A complete picture of the GM cooling is described in detail in [40],

taking into account the full Zeeman-level structure. More recently, GM cooling has been widely realized on many alkali atomic species operating on the D_1 transition [41–45], and even successfully implemented on the D_2 transition [31,46–49].

The cooling, repumping, and GM light is provided by a master oscillator + Raman fiber amplifier + frequency doubling system with an output of 2 W at 589 nm. This power is sufficient for cooling and trapping of ^{23}Na in our experiment. This single laser source supplies the coherence between the two frequencies to generate the long-lived dressed dark states in the GM cooling. The cooling and repumping laser frequencies are finely adjusted using acousto-optic modulators (AOMs) in the double-pass configuration [50]. In the GM cooling stage, the cooling and repumper frequencies are tuned to Δ_{CG} and Δ_{RG}, as shown in Fig. 2, where the two-photon Raman detuning is defined as $\delta = \Delta_{RG} - \Delta_{CG}$. The AOMs act as fast switches and frequency and intensity tuners. After the frequency tuning, the cooling and repumping lights are combined by a polarization beam splitter (PBS) and then divided by several PBSs into six beams to be delivered to the science chamber by polarization-maintaining optical fibers.

After collecting atoms for 20 s in the 3D MOT, the compressed MOT (CMOT) stage follows for 30 ms, after which the magnetic field is reduced to zero in 100 μs. Then the GM is applied for a duration of 4.5 ms keeping $\delta = 0$ and $\Delta_{CG} = \Delta_{RG} = +2.48\Gamma$, where Γ is the natural linewidth of the D2 line, as shown in Fig. 2. The typical time sequence for laser frequencies and intensities is sketched in Figs. 3(a) and 3(b). After the GM cooling stage, a cold and dense atomic cloud of 3×10^8 atoms is achieved at a temperature of 56 μK. The dependence of the temperature on the detuning, the pulse time, and the intensity ratio between the cooling and repumping light have been described in detail in [31]. The minimum temperature in GM cooling is affected by the coherence of the dark states, which is strongly reduced by the stray magnetic fields, the fluctuation of the laser frequency, and the power ratio between the laser beams.

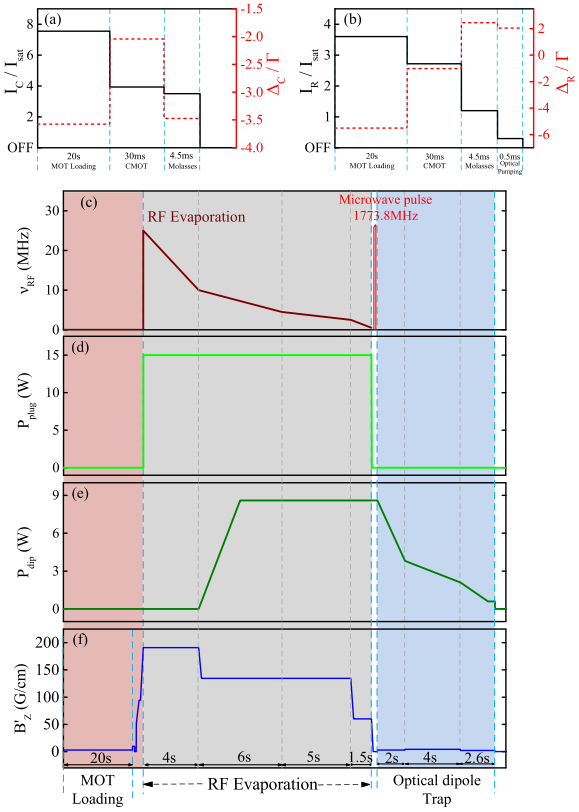

Fig. 3. Power I/I_{sat} and detuning Δ/Γ of (a) the trapping and (b) repumper laser beams as a function of time (Δ_R here represents the detuning from the $|F_g = 1\rangle \rightarrow |F_e = 2\rangle$ transition); (c) RF evaporation frequency; (d) optical plug beam; (e) power of the dipole trap beams; and (f) gradient of magnetic trap as a function of the sequence time during the MOT loading (red shaded region), RF evaporation in optically plugged magnetic trap (gray shaded region), and evaporation in optical trap (blue shaded region). A microwave (MW) pulse [red curve in (c)] is used to transfer the atoms to the lowest state $|1, 1\rangle$ after loading in to the optical trap when experiment is desired in the $|1, 1\rangle$ state.

4. EVAPORATIVE PRE-COOLING IN THE OPTICALLY PLUGGED MAGNETIC TRAP

In this section, the process of pre-cooling in the optically plugged magnetic trap using RF evaporation is described, whereas the entire time sequence of RF, the power of optical plug beam and crossed optical dipole trap beams, and the gradient of quadrupole magnetic trap is schematically shown in Figs. 3(c)–3(f). After the gray molasses stage, the atoms are optically pumped to the spin-polarized hyperfine state $|F = 2, m_F = 2\rangle$ by a σ^+ laser pulse of 0.5 ms at resonance with the $|F_g = 2\rangle \rightarrow |F_e = 2\rangle$ transition. In the pumping stage, the repumping light in the MOT beams is tuned to a blue detuning $\Delta_R = 2\Gamma$ to prevent the atoms from populating the $F = 1$ ground state.

Then, around 2.3×10^8 atoms at ∼250 μK are quickly loaded into the magnetic quadrupole trap at $B'_z = 90$ G/cm in 500 μs. The loading efficiency is about 76%, thanks to the lower temperature and high phase space density of the atomic cloud due to the GM technique. Loading the $|F = 2, m_F = 2\rangle$ ground state atoms into the magnetic trap is advantageous compared to the $F = 1$ ground state because the pumping process is not perfect and the atoms equally populate the three Zeeman sublevels in the $F = 1$ manifold. However, some techniques are developed to increase the pumping efficiency by optical pumping for the $|F = 1, m_F = -1\rangle$ state atoms in the presence of a high magnetic field [51].

Once the atoms are trapped in the magnetic trap, the gradient is increased to 199 G/cm in 100 ms to compress the atoms to high density, and then a blue-detuned 15 W laser at 532 nm laser light (Beijing Yuguang Science and Technology Development Co., Ltd., Beijing, China) is switched on and focused at the quadrupole magnetic trap center, creating a repulsive barrier to suppress the atomic Majorana losses. Thus, an optically plugged quadrupole magnetic trap is produced, with a total potential given by

$$U(x, y, z) = \mu B'_z \sqrt{\frac{x^2 + y^2}{4} + z^2} + U_p e^{-2\left(\frac{x^2+z^2}{\omega_0^2}\right)} - mgz, \quad (1)$$

where $\mu = \mu_B g_F m_F$ is the atomic magnetic moment, μ_B is the Bohr magneton, B'_z is the field gradient along z direction, $U_p = k_B \times 619\ \mu K$ is the depth of repulsive potential [52], $\omega_0 \approx 35\ \mu$m is the blue-detuned laser beam waist ($1/e^2$ radius), m is the mass of the sodium atom, and g is the acceleration of gravity.

After the loading of the sodium atoms in the $|2, 2\rangle$ state in the optically plugged quadrupole trap and waiting 100 ms to reach equilibrium, an RF-forced evaporative cooling is performed to cool the atoms down to 11 μK by a series of linear frequency sweeps from 25 MHz to 1.0–0.5 MHz in 16.5 s. Meanwhile, a two-step decompression of the magnetic field optimizes the phase space density (PSD) of the atomic sample [Fig. 3(f)] to reduce the three-body inelastic losses in the evaporation stage.

To optimize the evaporative cooling in the optically plugged magnetic trap, we compare the evaporation trajectories in three cases: in the quadrupole magnetic trap (orange triangles); in the optically plugged quadrupole magnetic trap with (red circles); and without (green circles) the decompression steps [gray portion in Fig. 4(a)] using the parameter $s = \log(N)/\log(T)$, which estimates the RF-evaporation efficiency. The evolution of the atom number versus temperature in the cooling trajectories is displayed in Fig. 4(a). The parameter s is obtained by the linear fit (the solid curves) to the experimental data. In the case of the optically plugged quadrupole magnetic trap (red circles), the fit gives an s value of 1.03, signifying the efficiency of our evaporation sequence of Fig. 3. This value is better than the $s = 1.15$ obtained from the fit to the green circles that represent the case without decompression steps. In the case of the evaporation only in the quadrupole magnetic trap, the linear fit gives $s = 2.99$ (orange triangles), which indicates that the Majorana losses reduce the RF-evaporation efficiency.

5. PRODUCTION OF ^{23}Na BEC IN THE OPTICAL TRAP

As a final step in the BEC production, an evaporation sequence is performed in the crossed optical dipole trap. To efficiently load the atoms in the far detuned optical trap (at 1064 nm), the crossed optical trap is located at one of the minima of the optically plugged magnetic trap. Each beam power reaches its maximum power of 9 W in a fast ramp at the start of the second RF-evaporation step, as shown in Fig. 3(e). At the crossing point, the two laser beams are focused to a waists of 107 μm and 70.5 μm, which produce a trap potential of depth $k_B \times 51$ μK. To improve the loading, the ring symmetry of the optically plugged quadrupole trap is broken by applying a homogeneous magnetic field along the y direction at the fourth step of RF evaporation, and a single minimum is generated to produce a high phase density atomic sample. After the loading, the magnetic field gradient is ramped down to zero in 30 ms and the plug beam is abruptly switched off. At this point, about 2.26×10^6 atoms in the $|2, 2\rangle$ state at 5.73 μK are trapped in the crossed optical trap with average trapping frequency $\varpi = (\omega_x\omega_y\omega_z)^{1/3} = 2\pi \times 442$ Hz. The sample temperature T and number N are estimated by taking absorption images after a few ms of time of flight (TOF), from which we obtain the peak density $n_p = \mathrm{N}\left(\frac{m\varpi^2}{2\pi k_B T}\right)^{3/2} = 3.26 \times 10^{13}\ \mathrm{cm}^{-3}$ and the peak phase-space density $\mathrm{D} = n_p\lambda_{dB}^3 \approx 1.15 \times 10^{-1}$, where $\lambda_{dB} = h/\sqrt{2\pi mk_B T}$ is the thermal de Broglie wavelength.

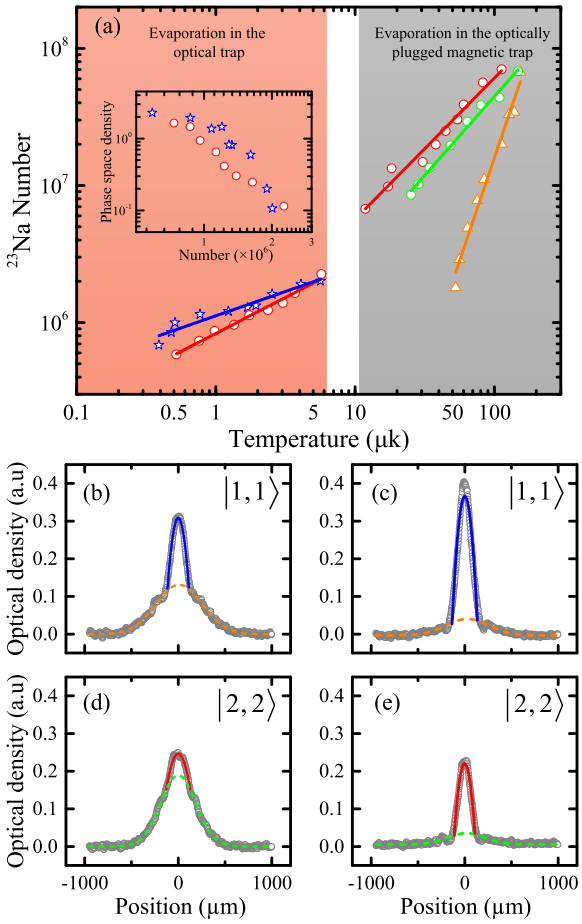

Fig. 4. (a) Evolution of the atom number N versus the temperature T during the evaporation in the magnetic trap (gray shaded region) and in the optical trap (red shaded region). The RF-evaporation in the optically plugged trap with (red circles) and without decompression (green circles) and the quadrupole magnetic trap only (orange triangles) are displayed in the gray shaded area. The evaporation of atoms in $|1, 1\rangle$ (blue stars) and $|2, 2\rangle$ (red circles) states in the optical trap are displayed in the red shaded area. Peak phase space density as a function of the atom number in the optical trap evaporation are shown in the inset image. The observed optical density (OD) along the x direction after 15 ms of TOF shows a bimodal momentum distribution in (b) and (d), and pure condensates in the two spin states after further evaporation (30 ms of TOF) in (c) and (e).

Using three steps of linear ramps to reduce the power in the optical trap beams, the depth of the optical dipole trap is reduced from 51 to 2.7 μK in 8.5 s, reaching the critical temperature. After an additional 100 ms of holding time in the optical trap, as shown in Fig. 3(f), a pure condensate of 2.5×10^5 atoms in the $|2, 2\rangle$ state is produced. The parabolic density profile measured after 30 ms TOF is displayed in Fig. 4. The peak density is calculated to be $9.18 \times 10^{13}\ \mathrm{cm}^{-3}$, where the s wave scattering length $a = 62.51a_0$ is used [53], a_0 being the Bohr radius. The depth of the trap in the final step of evaporation is $k_B \times 2.7$ μK and the trapping frequencies $(\omega_x, \omega_y, \omega_z) = 2\pi \times (72, 114, 134)$ Hz, are extracted by fitting the dipole model of the BEC in the harmonic trap. The

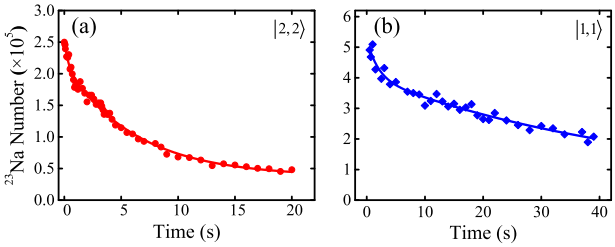

Fig. 5. Lifetime measurement of the sodium BEC in the (a) $|2, 2\rangle$ and (b) $|1, 1\rangle$ states. The solid lines show the numerical fits to the experimental data. The one-body loss fits give the BEC lifetimes of 6.3 ± 0.2 s for the $|2, 2\rangle$ state and 35.3 ± 7.6 s for the $|1, 1\rangle$ state.

whole route of evaporation in the optical dipole trap represented by the $N - T$ plane is shown in the red shaded area of Fig. 4.

To produce the condensate in the $|1, 1\rangle$ state, the atomic cloud in the optical dipole trap is transferred to the $|1, 1\rangle$ state by a microwave pulse (in the presence of a bias homogeneous magnetic field) after the quadrupole magnetic trap is switched off, as shown in Fig. 3(c). The microwave pulse is followed by an on-resonance laser flash of 2 ms to remove any residual atoms in $|2, 2\rangle$ state. Using a similar evaporation process in the dipole trap used for the atoms in $|2, 2\rangle$ state, a pure condensate of 5×10^5 atoms in the $|1, 1\rangle$ state is obtained, with a peak density of 1.34×10^{14} cm^{-3} for $a = 52.98a_0$ [53].

We compare the optical trap evaporation efficiency of atoms in the $|2, 2\rangle$ and $|1, 1\rangle$ states by the parameter s, obtained from the fit to the two evaporation trajectories shown in the red shaded area in Fig. 4(a). The value $s = 0.3546$ for $|1, 1\rangle$ state indicates a better collision rate and efficient evaporation compared to the $|2, 2\rangle$ state (with $s = 0.5252$), which can be attributed to the larger three-body loss rate in the $|2, 2\rangle$ state.

To analyze the collision properties of the atoms quantitatively in the two hyperfine states, we measure the time evolution of the atom number N in the BEC in $|1, 1\rangle$ and $|2, 2\rangle$ states by holding them in the optical trap for a variable hold time. As shown in Fig. 5, for a shorter hold time, we can see a rapid decay of the atom number for both cases, which can be attributed to the three-body recombination losses. At a longer hold time, an exponential decay induced by the one-body loss can be seen. In our experimental conditions, the two-body loss does not play the dominant role at the densities considered here due to the relatively small two-body dipolar loss rate. The decay curve for the number of atoms in the BEC can be modeled by

$$\frac{dN}{dt} = -k_1 N - k_3 N\langle n^2\rangle, \tag{2}$$

where k_1 is the one-body loss rate induced by the collisions with background gas and the photon scattering in the optical trap, k_3 is the three-body loss rate, $\langle n^i\rangle = 1/N \int n^{i+1} dV$ is the weighted average density in a harmonic trap, and $\langle n^2\rangle$ is related to the peak density by $\langle n^2\rangle = 8/21\, n_p^2$ for BEC.

Fitting the solution of Eq. (2) to the data in Fig. 5 yields $k_1 = 0.159 \pm 0.006\ \text{s}^{-1}$ and $k_3 = (9.21 \pm 1.45) \times 10^{-28}\ \text{cm}^6\text{s}^{-1}$ for the BEC in the $|2, 2\rangle$ state. On the other hand, the fitted data of atoms in the $|1, 1\rangle$ state gives $k_1 = 0.029 \pm 0.006\ \text{s}^{-1}$ and $k_3 = (1.33 \pm 0.39) \times 10^{-28}\ \text{cm}^6\ \text{s}^{-1}$. The three-body loss rate in our case for the atoms in the $|2, 2\rangle$ state is a factor of 6.9 bigger than for the atoms in the $|1, 1\rangle$ state. These values for the three-body loss are one order of magnitude larger than the previous values of [24,25] while the one-body loss values are almost the same. This maybe attributed to different trapping geometries of the optical traps used ($\omega_z/\omega_{x,y} \sim 50$ in the pancake trap [24] and $\sim$167 in the 1D optical lattice [25]). The one-body loss rate in the $|2, 2\rangle$ state is approximately six times larger than in the $|1, 1\rangle$ state. This difference in the one-body loss rate for the two spin states can be attributed to the residual (but larger compared to the $|1, 1\rangle$ state) three-body losses in the $|2, 2\rangle$ state, even at the lower atomic density after the longer holding time.

6. CONCLUSIONS

We have reported the direct production of ^{23}Na condensate (lifetime 6.3 s) of 2.5×10^5 atoms in the $|2, 2\rangle$ state using a compact experimental setup. Gray molasses cooling on the D_2 transition results in a low temperature of 56 μK, which provides a good starting point for two-stage evaporative cooling in a magnetic trap and an optical trap. RF-induced evaporative cooling is performed in the optically plugged quadrapole magnetic trap, where the Majorana losses of sodium atoms are strongly suppressed by a focused blue-detuned laser beam. An efficient evaporative cooling in the optical trap follows the quadrupole magnetic trap evaporation, cooling the atoms from 5.73 μK to the BEC temperature. Furthermore, we also study the collision properties of sodium and show the significantly different three-body loss rates in the $|2, 2\rangle$ and $|1, 1\rangle$ states in the BEC. We believe our method can be used to cool the atomic mixtures of sodium and other species and provide a platform to study spin-2 spinor condensates and the collision properties of sodium atoms in the $F = 2$ manifold.

Funding. Ministry of Science and Technology of the People's Republic of China (2016YFA0301602, 2018YFA0307601); National Natural Science Foundation of China (11804203, 11974224, 12004229, 12022406, 12034011, 92065108); Shanxi Key Subjects Construction (1331); The Program of Youth Sanjin Scholar.

Disclosures. The authors declare no conflicts of interest.

REFERENCES

1. I. Bloch, J. Dalibard, and W. Zwerger, "Many-body physics with ultracold gases," Rev. Mod. Phys. **80**, 885–964 (2008).
2. P. Windpassinger and K. Sengstock, "Engineering novel optical lattices," Rep. Prog. Phys. **76**, 086401 (2013).
3. A. Eckardt, "Colloquium: atomic quantum gases in periodically driven optical lattices," Rev. Mod. Phys. **89**, 011004 (2017).
4. C. Gross and I. Bloch, "Quantum simulations with ultracold atoms in optical lattices," Science **357**, 995–1001 (2017).
5. D.-W. Wang, H. Cai, L. Yuan, S.-Y. Zhu, and R.-B. Liu, "Topological phase transitions in superradiance lattices," Optica **2**, 712–715 (2015).
6. V. Galitski and I. B. Spielman, "Spin–orbit coupling in quantum gases," Nature **494**, 49–54 (2013).
7. H. Zhai, "Degenerate quantum gases with spin–orbit coupling: a review," Rep. Prog. Phys. **78**, 026001 (2015).
8. J. Zhang, H. Hu, X.-J. Liu, and H. Pu, "Fermi gases with synthetic spin–orbit coupling," Annu. Rev. Cold Atoms Mol. **2**, 81–143 (2014).
9. Z. Hu, C. Liu, J.-M. Liu, and Y. Wang, "Electromagnetically induced transparency in a spin-orbit coupled Bose-Einstein condensate," Opt. Express **26**, 20122–20131 (2018).

10. L. D. Carr, D. DeMille, R. V. Krems, and J. Ye, "Cold and ultracold molecules: science, technology and applications," New J. Phys. **11**, 055049 (2009).
11. S. A. Moses, J. P. Covey, M. T. Miecnikowski, D. S. Jin, and J. Ye, "New frontiers for quantum gases of polar molecules," Nat. Phys. **13**, 13–20 (2017).
12. C.-H. Wu, J. W. Park, P. Ahmadi, S. Will, and M. W. Zwierlein, "Ultracold fermionic Feshbach molecules of $^{23}Na^{40}K$," Phys. Rev. Lett. **109**, 085301 (2012).
13. F. Wang, X. He, X. Li, B. Zhu, J. Chen, and D. Wang, "Formation of ultracold NaRb Feshbach molecules," New J. Phys. **17**, 035003 (2015).
14. T. M. Rvachov, H. Son, A. T. Sommer, S. Ebadi, J. J. Park, M. W. Zwierlein, W. Ketterle, and A. O. Jamison, "Long-lived ultracold molecules with electric and magnetic dipole moments," Phys. Rev. Lett. **119**, 143001 (2017).
15. F. Seeßelberg, N. Buchheim, Z.-K. Lu, T. Schneider, X.-Y. Luo, E. Tiemann, I. Bloch, and C. Gohle, "Modeling the adiabatic creation of ultracold polar $^{23}Na^{40}K$ molecules," Phys. Rev. A **97**, 013405 (2018).
16. S. B. Papp, J. M. Pino, and C. E. Wieman, "Tunable miscibility in a dual-species Bose-Einstein condensate," Phys. Rev. Lett. **101**, 040402 (2008).
17. D. J. McCarron, H. W. Cho, D. L. Jenkin, M. P. Köppinger, and S. L. Cornish, "Dual-species Bose-Einstein condensate of ^{87}Rb and ^{133}Cs," Phys. Rev. A **84**, 011603 (2011).
18. L. Wacker, N. B. Jørgensen, D. Birkmose, R. Horchani, W. Ertmer, C. Klempt, N. Winter, J. Sherson, and J. J. Arlt, "Tunable dual-species Bose-Einstein condensates of ^{39}K and ^{87}Rb," Phys. Rev. A **92**, 053602 (2015).
19. A. T. Black, E. Gomez, L. D. Turner, S. Jung, and P. D. Lett, "Spinor dynamics in an antiferromagnetic spin-1 condensate," Phys. Rev. Lett. **99**, 070403 (2007).
20. Y. Kawaguchi and M. Ueda, "Spinor Bose-Einstein condensates," Phys. Rep. **520**, 253–381 (2012).
21. M. O. Borgh and J. Ruostekoski, "Core structure and non-Abelian reconnection of defects in a biaxial nematic spin-2 Bose-Einstein condensate," Phys. Rev. Lett. **117**, 275302 (2016).
22. T. Mawson, T. Petersen, J. Slingerland, and T. Simula, "Braiding and fusion of non-Abelian vortex anyons," Phys. Rev. Lett. **123**, 140404 (2019).
23. N.-S. Wan, Y.-E. Li, and J.-K. Xue, "Solitons in spin-orbit-coupled spin-2 spinor Bose-Einstein condensates," Phys. Rev. E **99**, 062220 (2019).
24. A. Görlitz, T. L. Gustavson, A. E. Leanhardt, R. Löw, A. P. Chikkatur, S. Gupta, S. Inouye, D. E. Pritchard, and W. Ketterle, "Sodium Bose-Einstein condensates in the F=2 state in a large-volume optical trap," Phys. Rev. Lett. **90**, 090401 (2003).
25. H. Imai, T. Akatsuka, T. Ode, and A. Morinaga, "Collisional loss rates of sodium Bose-Einstein condensates in the F=2 state in a one-dimensional optical lattice," Phys. Rev. A **85**, 013633 (2012).
26. J. W. Park, S. A. Will, and M. W. Zwierlein, "Ultracold dipolar gas of fermionic $^{23}Na^{40}K$ molecules in their absolute ground state," Phys. Rev. Lett. **114**, 205302 (2015).
27. P. S. Żuchowski and J. M. Hutson, "Reactions of ultracold alkali-metal dimers," Phys. Rev. A **81**, 060703 (2010).
28. A. Gerdes, M. Hobein, H. Knöckel, and E. Tiemann, "Ground state potentials of the NaK molecule," Eur. Phys. J. D **49**, 67–73 (2008).
29. J. W. Park, C.-H. Wu, I. Santiago, T. G. Tiecke, S. Will, P. Ahmadi, and M. W. Zwierlein, "Quantum degenerate Bose-Fermi mixture of chemically different atomic species with widely tunable interactions," Phys. Rev. A **85**, 051602 (2012).
30. H. Son, J. J. Park, W. Ketterle, and A. O. Jamison, "Collisional cooling of ultracold molecules," Nature **580**, 197–200 (2020).
31. Z. Shi, Z. Li, P. Wang, Z. Meng, L. Huang, and J. Zhang, "Sub-Doppler laser cooling of ^{23}Na in gray molasses on the D_2 line," Chin. Phys. Lett. **35**, 123701 (2018).
32. Z.-L. Li, Z.-L. Shi, and P.-J. Wang, "Design and research of two-dimensional magneto-optical trap of sodium atom using permanent magnets," Acta Phys. Sin. **69**, 126701 (2020).
33. T. G. Tiecke, S. D. Gensemer, A. Ludewig, and J. T. M. Walraven, "High-flux two-dimensional magneto-optical-trap source for cold lithium atoms," Phys. Rev. A **80**, 013409 (2009).
34. G. Lamporesi, S. Donadello, S. Serafini, and G. Ferrari, "Compact high-flux source of cold sodium atoms," Rev. Sci. Instrum. **84**, 063102 (2013).
35. K. Li, D. Zhang, T. Gao, S.-G. Peng, and K. Jiang, "Enhanced trapping of cold ^{6}Li using multiple-sideband cooling in a two-dimensional magneto-optical trap," Phys. Rev. A **92**, 013419 (2015).
36. H. Tanaka, H. Imai, K. Furuta, Y. Kato, S. Tashiro, M. Abe, R. Tajima, and A. Morinaga, "Dual magneto-optical trap of sodium atoms in ground hyperfine F = 1 and F = 2 states," Jpn. J. Appl. Phys. **46**, L492–L494 (2007).
37. A. Aspect, E. Arimondo, R. Kaiser, N. Vansteenkiste, and C. Cohen-Tannoudji, "Laser cooling below the one-photon recoil energy by velocity-selective coherent population trapping," Phys. Rev. Lett. **61**, 826–829 (1988).
38. L. Guidoni and P. Verkerk, "Optical lattices: cold atoms ordered by light," J. Opt. B **1**, R23–R45 (1999).
39. J. Dalibard and C. Cohen-Tannoudji, "Laser cooling below the Doppler limit by polarization gradients: simple theoretical models," J. Opt. Soc. Am. B **6**, 2023–2045 (1989).
40. F. Sievers, N. Kretzschmar, D. R. Fernandes, D. Suchet, M. Rabinovic, S. Wu, C. V. Parker, L. Khaykovich, C. Salomon, and F. Chevy, "Simultaneous sub-Doppler laser cooling of fermionic ^{6}Li and ^{40}K on the D_1 line: theory and experiment," Phys. Rev. A **91**, 023426 (2015).
41. D. R. Fernandes, F. Sievers, N. Kretzschmar, S. Wu, C. Salomon, and F. Chevy, "Sub-Doppler laser cooling of fermionic ^{40}K atoms in three-dimensional gray optical molasses," Europhys. Lett. **100**, 63001 (2012).
42. A. T. Grier, I. Ferrier-Barbut, B. S. Rem, M. Delehaye, L. Khaykovich, F. Chevy, and C. Salomon, "Λ-enhanced sub-Doppler cooling of lithium atoms in D_1 gray molasses," Phys. Rev. A **87**, 063411 (2013).
43. G. Salomon, L. Fouché, P. Wang, A. Aspect, P. Bouyer, and T. Bourdel, "Gray-molasses cooling of ^{39}K to a high phase-space density," Europhys. Lett. **104**, 63002 (2013).
44. A. Burchianti, G. Valtolina, J. A. Seman, E. Pace, M. De Pas, M. Inguscio, M. Zaccanti, and G. Roati, "Efficient all-optical production of large ^{6}Li quantum gases using D_1 gray-molasses cooling," Phys. Rev. A **90**, 043408 (2014).
45. G. Colzi, G. Durastante, E. Fava, S. Serafini, G. Lamporesi, and G. Ferrari, "Sub-Doppler cooling of sodium atoms in gray molasses," Phys. Rev. A **93**, 023421 (2016).
46. D. Zhang, Y.-Q. Li, Y.-F. Wang, Y.-M. Fu, P. Li, W.-L. Liu, J.-Z. Wu, J. Ma, L.-T. Xiao, and S.-T. Jia, "Enhanced optical molasses cooling for Cs atoms with largely detuned cooling lasers," Chin. Phys. B **29**, 23203 (2020).
47. G. D. Bruce, E. Haller, B. Peaudecerf, D. A. Cotta, M. Andia, S. Wu, M. Y. H. Johnson, B. W. Lovett, and S. Kuhr, "Sub-Doppler laser cooling of ^{40}K with Raman gray molasses on the D_2 line," J. Phys. B **50**, 095002 (2017).
48. S. Rosi, A. Burchianti, S. Conclave, D. S. Naik, G. Roati, C. Fort, and F. Minardi, "Λ-enhanced grey molasses on the D_2 transition of ^{87}Rb atoms," Sci. Rep. **8**, 1301 (2018).
49. Y.-F. Hsiao, Y.-J. Lin, and Y.-C. Chen, "Λ-enhanced gray-molasses cooling of cesium atoms on the D_2 line," Phys. Rev. A **98**, 033419 (2018).
50. E. A. Donley, T. P. Heavner, F. Levi, M. O. Tataw, and S. R. Jefferts, "Double-pass acousto-optic modulator system," Rev. Sci. Instrum. **76**, 063112 (2005).
51. K. M. R. van der Stam, A. Kuijk, R. Meppelink, J. M. Vogels, and P. van der Straten, "Spin-polarizing cold sodium atoms in a strong magnetic field," Phys. Rev. A **73**, 063412 (2006).
52. L.-C. Chen, Z.-M. Meng, and P.-J. Wang, "The rapid experimental preparation of ^{87}Rb Bose-Einstein condensate," Acta Phys. Sin. **66**, 083701 (2017).
53. C. Samuelis, E. Tiesinga, T. Laue, M. Elbs, H. Knöckel, and E. Tiemann, "Cold atomic collisions studied by molecular spectroscopy," Phys. Rev. A **63**, 012710 (2000).